Time-domain perspective on Autler-Townes splitting in attosecond transient absorption of laser-dressed helium atoms

Mengxi Wu, Shaohao Chen, Mette B. Gaarde, and Kenneth J. Schafer
Department of Physics and Astronomy, Louisiana State University, Baton Rouge, Louisiana 70803-4001, USA
(Received 21 June 2013; published 15 October 2013)

We present a theoretical study of the delay-dependent Autler-Townes (AT) splitting in transient absorption spectroscopy of an isolated attosecond pulse in helium atoms subject to a delayed infrared (IR) pulse. We concentrate on cases in which the IR pulse is resonant with the helium $1s2p$-$1s2s$ transition and provide a time-domain perspective of the dynamics in the delay-dependent pump-probe system. We identify several interesting delay-dependent features in the transient absorption spectrum such as AT splitting, oscillation between absorption and emission at the resonant absorption frequency, and sub-IR-cycles oscillations. We then explain the origins of these features in the time domain in terms of a strongly driven two-level system, in the language of population transfer and coherent control.

DOI: 10.1103/PhysRevA.88.043416 PACS number(s): 32.80.Qk, 32.70.Jz, 42.50.Hz, 42.50.Md

I. INTRODUCTION

Attosecond transient absorption uses a delay-dependent pump-probe scheme to investigate ultrafast electron dynamics down to the sub-femtosecond time scale [1,2]. The inherent waveform synchronization of a strong infrared (IR) laser probe pulse to an attosecond pump pulse produced via high harmonic generation [3–6] allows very high precision control of the delay time between them. In this way, a delay-dependent transient absorption spectrum can be obtained and the sub-femtosecond electron-photon dynamics can be retrieved. A wide range of ultrafast dynamics has been revealed using attosecond transient absorption, ranging from dielectric transitions in a semiconductor [7], to electron motion in the valence shell [1], and the relaxation dynamics of super excited oxygen [8], covering a variety of areas in physics, chemistry, material science, and biology [9], especially in attosecond transient absorption spectroscopy [10–17].

Our recent papers [14,15] have investigated the transient absorption spectrum in helium atoms, where we identified interesting interference features near the ionization threshold. In [14,15], the features in the absorption spectrum are mostly explained in the frequency domain, in the language of interfering contributions to the dipole moment corresponding to different excitation pathways. In this paper we will investigate the transient absorption dynamics in a time-domain picture, using the language of population transfer and coherent control. We focus on the transient absorption spectrum in the case of Autler-Townes (AT) splitting near the $1s^2$-$1s2p$ transition in atomic helium (21.1 eV). We show that the traditional AT splitting in a long IR pulse acquires rich absorption and emission features in the isolated attosecond pulse (IAP) + IR case, in addition to the two well-known absorption peaks [18]. The time-domain picture enables us to take advantage of the fact that the wave packet created by the IAP is essentially independent of the delay [15]. This allows us to separate the dynamics of the system into a slow part related only to the IR pulse and a fast part related only to the XUV pulse. By doing this separation, we are able to explain the transient absorption features in terms of a strongly driven two-level system. A similar time-domain treatment has been studied recently by Pfeiffer and Leone [18]. They presented an approximate analytical solution for a three-level model which can predict many of the features both within and beyond the rotating-wave approximation (RWA). In this paper, we focus on identifying the RWA and non-RWA features, studying how the weight of their relative contributions changes with IR intensity, and examining their dynamics using several different pulse shapes.

The paper is organized as follows. In Sec. II, we begin with the delay-dependent transient absorption spectrum calculated by solving the time-dependent Schrödinger equation (TDSE) for a helium atom, using the single active electron (SAE) approximation [19,20]. We identify several interesting features in the transient absorption spectrum and interpret them in terms of a strongly driven two-level system. We categorize these features into those that can be explained by the rotating-wave terms (RWTs), and those that can be explained by the counter-rotating terms (CRTs). In Sec. III, we focus on the RWT features and use several models to study the delay and frequency-dependent features that reveal how the familiar AT splitting spectrum is built up in the time domain. In Sec. IV, we study the effects of the CRTs and provide a simple model which can reproduce some of the CRT features in the transient absorption spectrum.

II. TRANSIENT ABSORPTION SPECTRUM

We start by showing the transient absorption spectrum of a helium atom, excited by an IAP with a full width at half maximum (FWHM) duration of 356 as and a central frequency at 25 eV, together with a four cycles IR pulse with a FWHM duration of 34 fs and a wavelength of 2550 nm. The XUV field has an intensity of 1.0×10^{11} W/cm^2, and the IR laser has an intensity of 3.0×10^{12} W/cm^2. At this intensity, net population excited from the ground state by the IR pulse can be ignored compared to that excited by the XUV pulse. The helium $1s2p$-$1s2s$ states are resonantly coupled by the IR laser. We solve the TDSE in the SAE approximation to obtain the time-dependent dipole moment using a pseudopotential [21]. The single atom absorption spectrum is calculated by a response function [21]

$$\tilde{S}(\omega) = -2\,\mathrm{Im}[\tilde{d}(\omega)\tilde{\mathcal{E}}^*(\omega)], \tag{1}$$

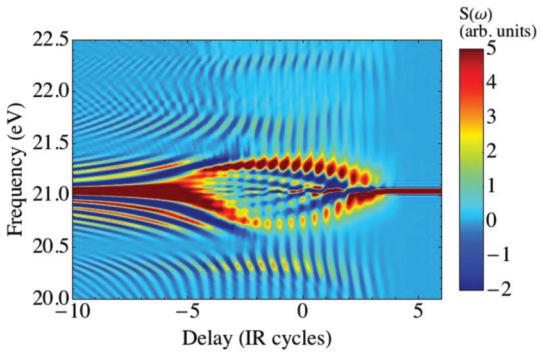

FIG. 1. (Color online) Full TDSE calculation of the transient absorption spectrum. The XUV pulse has a FWHM duration of 356 as, centered at 25 eV. The IR pulse has a duration of 34 fs and a wavelength 2550 nm, which is resonant with the $1s2p$-$1s2s$ transition.

where $\tilde{d}(\omega)$ and $\tilde{\mathcal{E}}(\omega)$ are the Fourier transforms of the time-dependent dipole and the electric field.[1] This response function represents the absorption probability density at a certain frequency, so that positive (negative) $\omega\tilde{S}(\omega)$ equals the amount of energy gained (lost) by the atom per unit frequency at ω. In calculating $\tilde{d}(\omega)$ we have included a dipole dephasing time of $T_2 = 136$ fs in $d(t)$. The dephasing serves the dual purpose of (i) taking into account spontaneous decay and collisional broadening that would be present in an experiment, and (ii) ensuring that $d(t)$ goes smoothly to zero at the end of the calculation. We have verified that using a longer T_2 does not change any of our conclusions.

The delay-dependent absorption spectrum calculated by Eq. (1) is shown in Fig. 1. From the absorption spectrum we can see several interesting features. The most dominant one is the forklike structure around 21.1 eV, where the $2p$ absorption line is split into two curved lines above and below the resonant frequency when the XUV and IR overlap. This structure is very similar to the ordinary AT splitting structure except the spacing between the two features depends on the IR intensity and thus changes with delay as the delay is scanned. Inside the AT splitting structure, there are also forklike structures going from positive to negative delays. Moreover, at large negative delays ($\tau < -5$), where the XUV pulse leads the IR pulse, there are hyperbolic sidebands near the $2p$ resonant line. These structures have also been seen recently in the absorption spectrum of a laser coupled autoionizing system [16]. In addition, in the region above and below the main AT splitting structure, namely above 21.5 eV and below 20.5 eV, we can see stripes across the delay scan. We will show that most of these structures can be understood by considering a strongly driven two-level system exhibiting both RWT and CRT behavior.

III. EFFECTS OF ROTATING-WAVE TERM

A. Move into the RWA regime

In the transient absorption scheme we study, the IR pulse is resonant with the helium $2p$-$2s$ energy, so that the atomic response near 21 eV is dominated by the $1s$-$2s$-$2p$ three level dynamics (we drop the $1s$ label from the states from now on as we will be working exclusively in the SAE approximation). In this sense, we can use only the lowest three levels $1s$-$2p$-$2s$ to approximate the dynamics of the field and the helium atom, ignoring all the higher-energy states [14]. Moreover, since the XUV pulse is short and weak in our case, we can approximate it as a δ function with its strength proportional to the pulse area of the full XUV field. With these approximations, the effects of the XUV and IR pulse on the atom are separated in the time domain: the XUV pulse will suddenly populate the $2p$ state and then the IR pulse will manipulate the $2p$ population by coupling it to the $2s$ state afterwards. After the $2p$ state is populated at time $t = 0$, the $1s$-$2p$ dipole will continue "ringing"at its natural frequency until the dipole dephases. In addition to that fast oscillation, the IR pulse will modify the $2p$ population on a much slower time scale. Thus the time-dependent dipole moment can be separated into a component that oscillates at the $1s$-$2p$ frequency ω_0 (after the XUV pulse), and a component $f(t)$ due to the manipulation of the $2p$ population by the IR field,

$$d(t) = f(t)e^{i\omega_0 t} + \text{c.c.} \tag{2}$$

This is shown in Fig. 2, where ω_0 is the resonant frequency of the $1s$-$2p$ transition. We have assumed the XUV pulse is located at $t = 0$.

The absorption spectrum, which is related to the Fourier transform of the time-dependent dipole moment, is basically determined by the IR manipulation part $f(t)$ with a spectral shift of ω_0. Thus the three-level two-field problem is further simplified to a two-level one-field problem, with only the $2p$ and $2s$ states and the IR field involved. The two-level system is described by the equations

$$i\dot{C}_{2s} = \mu_1 \mathcal{E}_{IR}(t,\tau)e^{-i\omega_1 t}C_{2p}, \tag{3a}$$

$$i\dot{C}_{2p} = \mu_1 \mathcal{E}_{IR}(t,\tau)e^{i\omega_1 t}C_{2s}, \tag{3b}$$

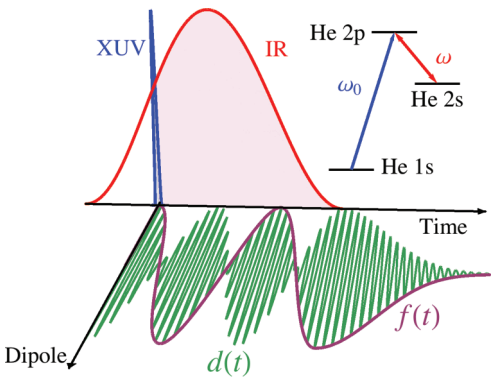

FIG. 2. (Color online) Schematic representation of our transient absorption model. The XUV pulse starts the dipole oscillation of the atom. The time-dependent dipole $d(t)$ contains both the fast oscillation at the $1s$-$2p$ transition frequency ω_0, and the slow oscillation $f(t)$, which is determined solely by the residual part (pink area) of the IR pulse. Since the fast oscillation gives only a translation in the frequency domain, the shape of the absorption spectrum is exclusively determined by the slow modulation.

[1]Note that the choice of Fourier transform convention determines the sign in Eq. (1). In this paper we use $\tilde{d}(\omega) = \frac{1}{\sqrt{2\pi}}\int_{-\infty}^{\infty} d(t)e^{-i\omega t}dt$, which gives the minus sign shown.

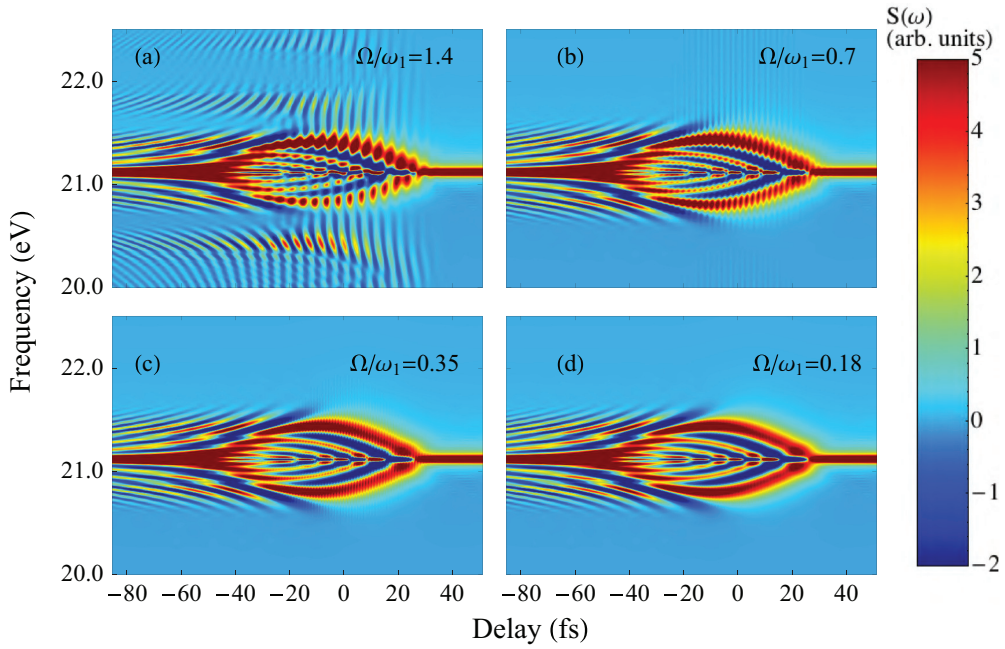

FIG. 3. (Color online) Stepping into the RWA regime as we decrease the ratio Ω/ω_1. Absorption spectrum calculated by Eq. (3) using (a) the original $\Omega/\omega_1 = 1.4$, (b) $\Omega/\omega_1 = 0.7$, (c) $\Omega/\omega_1 = 0.35$, and (d) $\Omega/\omega_1 = 0.18$. The non-RWA features such as subcycle oscillations and stripes are eliminated, while the RWA features of the main AT splitting are preserved.

with initial condition

$$C_{2s}(0) = 0, \tag{4a}$$

$$C_{2p}(0) = C^0_{2p}, \tag{4b}$$

where C_{2s} and C_{2p} represent the $2s$ and $2p$ amplitudes in the rotating frame, respectively. ω_1 is the $2p$-$2s$ transition frequency, which is also the IR frequency since in our case the IR pulse is always resonant with the $2p$-$2s$ transition. C^0_{2p} is the initial $2p$ population just after the XUV has passed, and is proportional to the XUV pulse area. $\mathcal{E}_{IR}(t,\tau)$ is the time- and delay-dependent IR field. μ_1 is the dipole transition element between the $2s$ and $2p$ states. The absorption spectrum resulting from this two-level model is shown in Fig. 3(a) and is in very good agreement with the full TDSE calculation in Fig. 1.

The model calculation in Fig. 3(a) encompasses effects of both RWTs and CRTs. This is in part because the IR field is relatively strong so that the RWA is not well defined. Using the dipole matrix elements from the same potential as the full calculation in Fig. 1, we can calculate the peak Rabi frequency Ω is 0.7 eV at an IR intensity of 3.0×10^{12} W/cm^2. This Rabi frequency is larger than the $2p$-$2s$ frequency of 0.5 eV, and the RWA weak-coupling condition is therefore not fulfilled [22]. In Figs. 3(b)–3(d), we explore features in Fig. 3(a) which can be attributed to RWTs, by gradually decreasing the ratio Ω/ω_1. This is done by increasing the IR carrier frequency while keeping the Rabi frequency fixed to maintain the same coupling strength. Since we want to keep the IR field resonant with the $2p$-$2s$ transition, we also increase the $2p$-$2s$ energy difference at the same time as we increase the IR carrier frequency. Figures 3(b)–3(d) then show that the delay-dependent AT-splitting peaks, the forklike structures inside the AT peaks, and the hyperbolic sidebands are all due to the RWTs, whereas the subcycle oscillations and the "stripes" above and below the main features are eliminated in the RWA regime.

B. Trigonometric envelope IR pulse

In this section, we study the RWA features in the absorption spectrum by analytically solving the two-level TDSE in the RWA, which reads [23,24]

$$i\dot{C}_{2s} = \tfrac{1}{2}\Omega(t,\tau)C_{2p}, \tag{5a}$$

$$i\dot{C}_{2p} = \tfrac{1}{2}\Omega(t,\tau)C_{2s}, \tag{5b}$$

where $\Omega(t,\tau)$ is the time- and delay-dependent envelope of the IR pulse multiplied by the dipole transition element μ_1. The above equations have a closed-form solution for a trigonometric envelope ($\cos^2$ or $\sin^2$) for delays when the XUV and IR pulses overlap (see Appendix A):

$$C_{2p}(t,\tau) = C^0_{2p}\cos\left[\frac{\Omega_0}{4\omega_1}\left(\omega_1 t + n\sin\frac{\omega_1\tau}{n} + n\sin\frac{\omega_1(t-\tau)}{n}\right)\right], \tag{6}$$

where τ is the delay between the centers of the XUV and IR pulses, n is the total number of cycles in the full IR pulse, and Ω_0 is the Rabi frequency corresponding to the peak IR intensity. C^0_{2p} is the initial $2p$ population just after the XUV has passed, which is proportional to the XUV pulse area. Using the above equation, we can calculate the response function

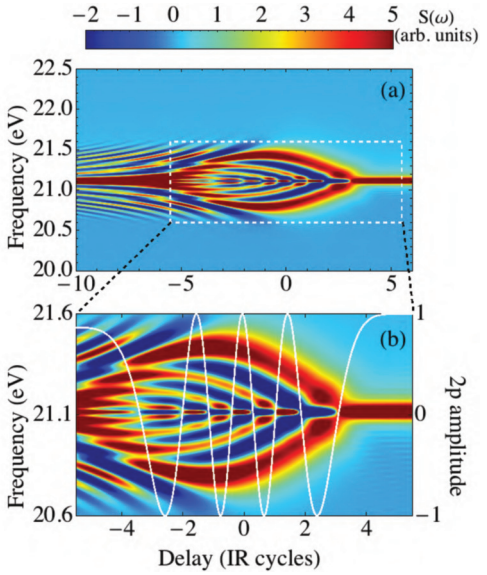

FIG. 4. (Color online) (a) Response function calculated directly from Eq. (6). (b) Closeup from (a), showing that the Rabi oscillation at the resonant line matches with the oscillation of the final $2p$ state amplitude (white line).

directly, which is shown in Fig. 4(a). It looks very similar to Fig. 3(d). The final-state amplitude at the end of the IR pulse can also be written down, as a function of delay:

$$C_{2p}^{f}(\tau) = C_{2p}^{0}\cos\left\{\frac{\Omega_0}{4\omega_1}\left(n\pi + \omega_1\tau + n\sin\left[\frac{\omega_1\tau}{n}\right]\right)\right\}. \quad (7)$$

A plot of Eq. (7) (normalized) is shown in Fig. 4(b) overlayed in white on the absorption spectrum. We see from Fig. 4(b) that the final-state amplitude oscillates between positive and negative values, which matches well to the oscillation of the response function between absorption and emission on the $2p$ resonant line at 21.1 eV. This oscillation in final-state amplitude comes from the fact that as we are scanning the XUV pulse, the remaining IR pulse area will change as a function of delay. This causes the response function to oscillate between absorption (when the $2p$ amplitude at the end of the IR pulse is large and positive) and emission (when the $2p$ amplitude at the end of the IR pulse is large and negative). A similar reversal of absorption to emission by manipulating the coherence is also seen in our earlier paper on absorption in laser-dressed helium atoms [25]. In the earlier work, however, we studied a very different configuration, using a long, resonant XUV pulse and a short IR control pulse.

C. Square envelope IR pulse

Next, we explore the RWA structures even further by simplifying the model to consider a square IR pulse envelope in the RWA regime. As shown below, this enables us to write out an explicit expression for the response function. We ignore the sudden turn on and off effect of the IR pulse and directly model the effect of the IR pulse as purely a Rabi cycling of the $2p$-$2s$ population. The amplitude of the $2p$ state as a function of time can be written as follows.

When the XUV and IR pulses overlap,

$$C_{2p}(t) = \begin{cases} C_{2p}^{0}\cos\frac{\Omega t}{2}, & 0 < t < \tau_2, \\ C_{2p}^{0}\cos\frac{\Omega\tau_2}{2}, & \tau_2 \leqslant t, \end{cases} \quad (8)$$

and when the XUV leads the IR pulse,

$$C_{2p}(t) = \begin{cases} C_{2p}^{0}, & t < \tau_1, \\ C_{2p}^{0}\cos\frac{\Omega(t-\tau_1)}{2}, & \tau_1 \leqslant t < \tau_2, \\ C_{2p}^{0}\cos\frac{\Omega\tau_0}{2}, & \tau_2 \leqslant t, \end{cases} \quad (9)$$

where Ω is the IR Rabi frequency, which is a constant in this case. τ_1 and τ_2 are the start and end of the IR pulse and $\tau_2 - \tau_1$ equals the duration of the IR pulse τ_0. The delay scan is characterized by varying τ which is defined as the delay between the center of the XUV and IR pulses, so that $\tau = -(\tau_1 + \frac{\tau_0}{2})$. As in the case of the trigonometric envelope, a negative delay means that the XUV arrives before the center of the IR pulse.

After writing down the state amplitude, we can calculate the time-dependent dipole moment and the response function. After a short derivation (see Appendix B), we get the delay-dependent response function $\tilde{S}$ in these two cases (constant factors are omitted).

When the XUV and IR pulses overlap,

$$\begin{aligned}\tilde{S}(\omega,\tau) = {} & \frac{\tau_1+\tau_0}{2}\mathrm{sinc}\left[(\tau_1+\tau_0)\left(\Delta+\frac{\Omega}{2}\right)\right] \\ & + \frac{\tau_1+\tau_0}{2}\mathrm{sinc}\left[(\tau_1+\tau_0)\left(\Delta-\frac{\Omega}{2}\right)\right] \\ & + \cos\frac{\Omega(\tau_1+\tau_0)}{2}e^{-\alpha(\tau_1+\tau_0)} \\ & \times \mathrm{Re}\left[\frac{\alpha - i\Delta}{\alpha^2+\Delta^2}e^{-i\Delta(\tau_1+\tau_0)}\right], \end{aligned} \quad (10)$$

and when the XUV pulse leads the IR pulse,

$$\begin{aligned}\tilde{S}(\omega,\tau) & \\ = {} & \tau_1\mathrm{sinc}(\Delta\tau_1) \\ & + \frac{\tau_0}{2}\cos\left[\Delta\tau_1 + \frac{\tau_0}{2}\left(\Delta+\frac{\Omega}{2}\right)\right]\mathrm{sinc}\left[\frac{\tau_0}{2}\left(\Delta+\frac{\Omega}{2}\right)\right] \\ & + \frac{\tau_0}{2}\cos\left[\Delta\tau_1 + \frac{\tau_0}{2}\left(\Delta-\frac{\Omega}{2}\right)\right]\mathrm{sinc}\left[\frac{\tau_0}{2}\left(\Delta-\frac{\Omega}{2}\right)\right] \\ & + \cos\frac{\Omega\tau_0}{2}e^{-\alpha(\tau_0+\tau_1)}\mathrm{Re}\left[e^{-i\Delta(\tau_0+\tau_1)}\frac{\alpha-i\Delta}{\alpha^2+\Delta^2}\right]. \end{aligned} \quad (11)$$

In these equations, $\Delta = \omega - \omega_0$, $\tau_1 = -(\tau + \frac{\tau_0}{2})$, and $\alpha \approx \frac{1}{T_2}$ is the decoherence factor.

Figure 5(a) shows the delay dependence of the response function of a 93 fs square IR pulse (the same full length as the trigonometric pulse case) using these equations. Other parameters are identical to that in Fig. 3(a). We can see many similarities between the square pulse result and the RWA result of the trigonometric pulse case in Fig. 4(a). First of all, the response function around the resonant frequency oscillates between absorption and emission with a period of one-half of the Rabi cycles. We note that the oscillation period in the square IR case is exactly one-half Rabi period, whereas the period in the trigonometric pulse case is approximately the averaged

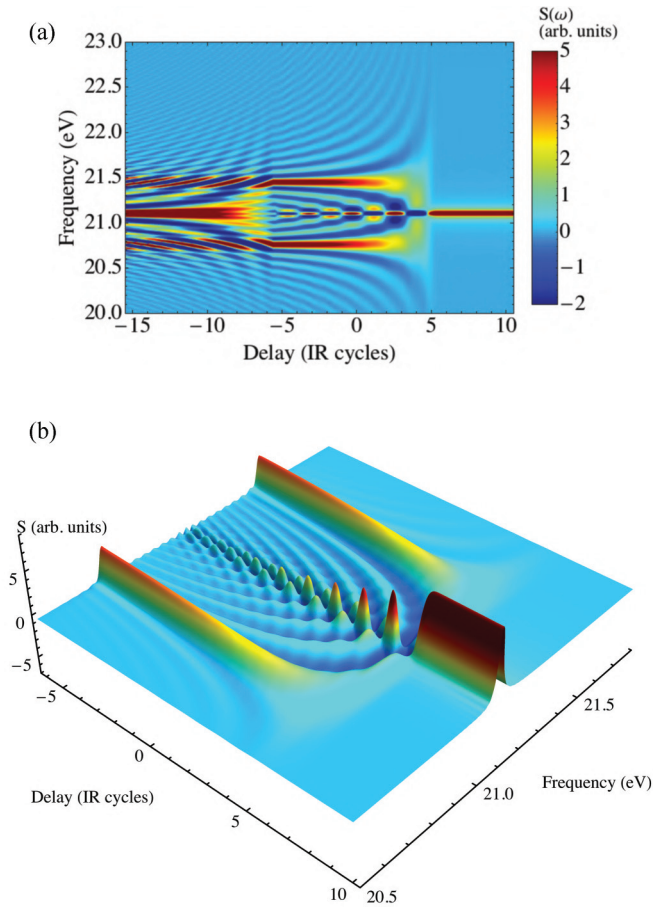

FIG. 5. (Color online) (a) Response function of the square IR pulse calculated from Eq. (10) and Eq. (11). We see similar features as for the trigonometric pulse case shown in Fig. 3(d) and Fig. 4(a). (b) The formation of the AT splitting structure, starting from a resonant (Lorentzian) line shape, as the atom experiences more and more cycles of the trapezoidal IR pulse, starting from large positive delays. Zero delay corresponds to the center of the IR pulse overlapping with the XUV pulse.

instantaneous Rabi period, such that it has a larger period in the beginning and end of the pulse and a smaller period in the center of the pulse. Second, in both cases, we have nested forklike structures, one inside another. In the square IR case, the fork structure consists of little steps, and is almost straight, while in the pulse case, the fork structure follows the IR pulse shape. Third, at about delay $\tau = -5$, there is a broomlike structure in both cases. Finally, at large negative delays ($\tau < -6$), there are stripes at the AT splitting lines, on top of which there are sinclike sideband structures.

Now we will use the model in Eqs. (10) and (11) to explain the structures of Fig. 5(a). We first study the features when the XUV and IR pulses overlap, in the region $-5.5 < \tau < 5.5$. In this case, the response function is described by Eq. (10). It contains three terms: the first two terms are from the contribution of the time interval when the IR pulse is on (from $0 \leqslant t \leqslant \tau_2$) and the third term is from the contribution of the dipole "ringing"after the IR pulse is over ($t > \tau_2$). We can see from Eq. (10) that the first and second terms are both sinc functions, which give rise to the two absorption peaks located at $\omega_0 \pm \Omega/2$ and their interference gives the forklike structures inside. We note that as the IR pulse duration gets longer, the sinc function will compress to a narrower frequency region. This weakens the inner structure compared to the main structure. In the limit of a continuous-wave IR pulse, these two sinc functions will collapse into two δ functions located at $\omega_0 \pm \Omega/2$, and there will be no inner structure, in agreement with the ordinary AT splitting. The curving of the main AT structure with delay was also predicted in [18], but in that work the inner structures are very faint because the IR intensity is high and the two main AT features are therefore separated further and interfere less. We can also see from Eq. (10) that at the resonant frequency 21.1 eV ($\Delta = 0$), the absorption is dominated by the dipole ringing term $\frac{1}{\alpha}\cos\frac{\Omega(\tau_1+\tau_0)}{2}e^{-\alpha(\tau_1+\tau_0)}$. This term results from the combined effect of a Rabi cycles oscillation term $\cos\frac{\Omega(\tau_1+\tau_0)}{2}$ and a ringing decay term $e^{-\alpha(\tau_1+\tau_0)}$.

Next we study the case when the XUV is leading the IR ($\tau < -5.5$), which is described by Eq. (11). In this case, the response function contains four terms. The first term comes from the contribution of the waiting time between XUV start and IR start ($0 \leqslant t \leqslant \tau_1$), the second and the third terms are the IR Rabi cycling term ($\tau_1 \leqslant t \leqslant \tau_2$), and the fourth term comes from the dipole ringing after the IR pulse is over ($t > \tau_2$). When $\tau < -5.5$, the IR manipulation of the population doesn't change with delay. The only thing that does change when scanning the delay is the waiting time between the arrival of the XUV pulse and that of the IR pulse. This has two effects. First, during this waiting time, the dipole will oscillate at the $1s$-$2p$ natural frequency, which gives a large absorption contribution at the $2p$ line at 21.1 eV, as we can see from both the first term in Eq. (11) and Fig. 5(a). Second, it will introduce a time translation of the IR manipulation (Rabi cycling) and thus introduce a delay-dependent phase to the absorption spectrum created by the IR pulse. This can also be seen by comparing the second and third terms in Eq. (11) to the first two terms in Eq. (10). This delay-dependent phase will change the AT absorption lines into delay-dependent stripes, as we see at around 20.7 eV and 21.5 eV in large negative delay in both the square IR pulse and the trigonometric IR pulse cases. A similar phenomenon was also reported in recent experiments by Ott *et al.* in [26], where they demonstrated that the transient absorption lineouts can change from Lorentzian to Fano shape by varying this delay-dependent phase.

Finally, in Fig. 5(b) we use a trapezoidal IR pulse to illustrate how the characteristic AT splitting structure is built up in the time domain. The response function is calculated within the RWA for a 130 fs trapezoidal IR pulse, which has two cycles for the turn on and turn off, and 11 cycles of the peak intensity. At large positive delay ($\tau > 5.5$), the IR pulse is leading the XUV pulse and has no effect on modifying the absorption; thus the absorption line has a regular Lorentzian shape. At $\tau \approx 5.5$, the atom starts to experience a few cycles of the IR pulse before it ends, and the Lorentzian line shape changes into complicated structures involving both absorption and emission as discussed above. At large negative delay ($\tau < -5.5$), as the atom experiences more cycles of the IR pulse, the AT splitting peaks start to build up and the inner structures start to disappear. The overall delay scan gives a clear indication of how the AT

splitting is formed from the Lorentzian line shape. We note that it is the combination of the few-cycles IR pulse and its subcycle synchronization to the XUV pulse that allows for probing the dynamics of the AT feature. A similar proposal for studying the evolution of the well-known Fano line shape of autoionizing states has recently appeared in [27].

IV. EFFECT OF COUNTER-ROTATING TERM

A. Subcycle oscillations

The full TDSE calculation in Fig. 1 shows that there are subcycle features that appear across the delay-dependent spectrum. These subcycle oscillations have been seen recently in transient absorption experiments [12,13,17]. In this section, we will focus on these subcycle oscillation features. From Fig. 3 we can see that when we move the system into the RWA regime, the subcycle features disappear while the main AT structure remains. This means the subcycle oscillations are related to the CRTs. We can investigate the strength and frequency of these subcycle oscillations by following the maximum value of the response function along the AT splitting line. The result is shown in Fig. 6, where the subcycle oscillation in the absorption along the AT splitting line is shown for four different Ω/ω_1 ratios, the same as in Fig. 3. Figure 6 shows that the frequency of these oscillations is approximately $2\omega_1$, and their modulation depth is basically proportional to Ω/ω_1 as one would expect from the RWA. The stripes above and below the main AT splitting are also from the CRTs. To explicitly study these CRT effects, one would need an approximate analytical solution containing the CRT terms, which has proven to be a very difficult task in general [28,29]. Here we use a crude model of the $2\omega_1$ effect.

We have the analytical solution of the trigonometric pulse under the RWA in Sec. III B. We may try to add the effects of the CRT directly into that solution. Since the CRTs have a $2\omega_1$ effect as we see in Fig. 6, we could model the CRT effects by adding a term $\sin(2\omega_1 t)$ directly into the time-dependent state amplitude. As we have seen, the strength of the CRTs may be characterized approximately by the ratio Ω/ω_1, since strong

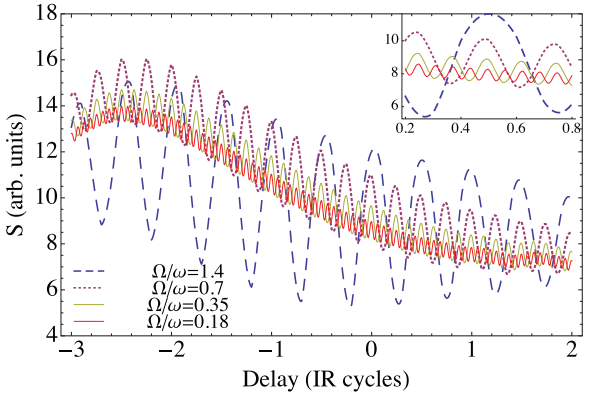

FIG. 6. (Color online) Subcycle oscillation retrieved from the absorption spectrum, by following the center of the AT splitting absorption line, in four different Ω/ω_1 ratios in Fig. 3. The figure shows that the subcycle oscillation strength is basically proportional to the carrier frequency, and the oscillation frequency is about two times the carrier frequency.

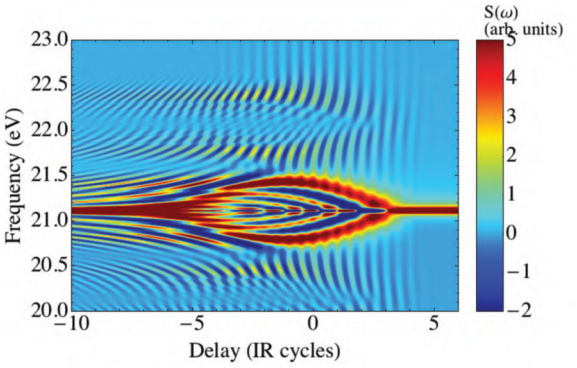

FIG. 7. (Color online) Adding $2\omega_1$ oscillation directly into the time-dependent state amplitude [Eq. (12)] reproduces the subcycle oscillation and the delay-dependent stripes. These stripes can be explained as a result of frequency mixing in the dipole oscillation.

coupling results in large CRT effects. Combining all of these estimates, we get a model time-dependent $2p$ amplitude:

$$C_{2p}(t,\tau) = C_{2p}^0 \cos\left[\frac{\Omega_0}{4\omega_1}\left(\omega_1 t + n\sin\frac{\tau\omega_1}{n} + n\sin\frac{\omega_1(t-\tau)}{n}\right)\right] \times\left(1+\beta\frac{\Omega(t,\tau)}{\omega_1}\sin[2\omega_1(t-\tau)]\right), \quad (12)$$

where $\Omega(t,\tau)=\cos^2[\frac{\omega_1(t-\tau)}{2n}]$ is the time- and delay-dependent Rabi frequency, and β is a free parameter which we take to be $1/2$.

Using Eq. (12), we can get a model response function, as shown in Fig. 7. We can see that by putting in a $2\omega_1$ oscillation directly into the state amplitude, the model can reproduce the striped structure outside the main AT splitting region. These stripes appears at $2\omega_1$ difference from the AT splitting (at about $\omega_0 \pm 2\omega_1 \pm \Omega_0/2$), which is reasonable since they represent the frequency mixing of the $\Omega/2$ and $2\omega_1$ components in the time-dependent dipole. Absorption (and emission) is possible at these frequencies because they are all within the broad bandwidth of the IAP. Adding the $2\omega_1$ component by hand to the state amplitude also generally reproduces the tilt of the subcycle oscillations, with a positive (negative) tilt of the stripes above (below) the AT structure. This is because the subcycle oscillations originate in an interference between the excitations that are separated by $2\omega_1$; see for instance [15]. These excitations result directly from adding the (lowest-order nonlinear) $2\omega_1$ term to C_{2p}. We note, though, that since the simple model incorporates neither higher-order terms nor the change of the effective Rabi frequency, it does not agree quantitatively with the numerical solution of the two-level system in Fig. 3(a), particularly on the phase of the fringes.

V. SUMMARY

We have studied the absorption of an IAP in the presence of an ultrafast, delayed IR pulse which strongly couples two excited states. We found that this system presents rich dynamics on the time scale of the IR pulse duration (tens of femtoseconds in our case), especially when the IR intensity is

high enough that several Rabi periods are completed within the duration of the pulse.

We have shown that the well-known Autler-Townes splitting of an absorption line in the presence of a resonant coupling field generalizes and becomes delay dependent when the coupling pulse is short. We also found prominent, delay-dependent interference features which lead to both absorption and emission within the AT structure. We showed that the dynamics of this delay dependence can be understood from the time-dependent population dynamics of a strongly driven two-level system. We also discussed how the formation of the AT splitting structure from the regular Lorentzian line shape can be probed in the scenario studied here, in which an attosecond XUV pulse is synchronized to the few-cycles pulse that causes the AT splitting.

Finally, we showed that although the main AT structure and its delay dependence are well described within the rotating-wave approximation, the full delay-dependent absorption spectrum is strongly influenced by counter-rotating terms which give rise to sub-IR-cycle oscillations as well as additional absorption lines corresponding to nonlinear mixing of the IR frequency and the Rabi frequency.

ACKNOWLEDGMENTS

This work was supported by the National Science Foundation under Grants No. PHY-0701372 and No. PHY-1019071. High-performance computational resources were provided by Louisiana State University and Louisiana Optical Network Initiative.

APPENDIX A: TRIGONOMETRIC IR PULSE

The simplified two-level equation in the RWA reads

$$i\dot{C}_{2s} = \tfrac{1}{2}\Omega(t,\tau)C_{2p}, \tag{A1a}$$

$$i\dot{C}_{2p} = \tfrac{1}{2}\Omega(t,\tau)C_{2s}, \tag{A1b}$$

with the initial condition of

$$C_{2s}(0,\tau) = 0, \tag{A2a}$$

$$C_{2p}(0,\tau) = C^0_{2p}, \tag{A2b}$$

where C^0_{2p} is the initial $2p$ population just after the XUV has passed. Since the XUV is weak, C^0_{2p} can be approximated as a pure imaginary number. This equation has the following solutions:

$$C_{2s}(t,\tau) = -iC^0_{2p}\sin\frac{\phi(t,\tau)}{2}, \tag{A3a}$$

$$C_{2p}(t,\tau) = C^0_{2p}\cos\frac{\phi(t,\tau)}{2}, \tag{A3b}$$

where

$$\phi(t,\tau) = \int_0^t \Omega(t',\tau)dt'. \tag{A4}$$

When the IR pulse has an envelope of $\cos^2$, the delay-dependent IR field is

$$\mathcal{E}_{\rm IR}(t,\tau) = \begin{cases} \mathcal{E}^0_{\rm IR}\cos^2\frac{\omega_1(t-\tau)}{2n}\sin\left[\omega_1(t-\tau)\right], & 0 \leqslant t \leqslant \frac{\pi n}{\omega_1}+\tau, \\ 0, & \frac{\pi n}{\omega_1}+\tau < t \end{cases} \tag{A5}$$

and $\Omega(t,\tau)$ is the time- and delay-dependent Rabi frequency

$$\Omega(t,\tau) = \begin{cases} \Omega_0\cos^2\frac{\omega_1(t-\tau)}{2n}, & 0 \leqslant t \leqslant \frac{\pi n}{\omega_1}+\tau, \\ 0, & \frac{\pi n}{\omega_1}+\tau < t, \end{cases} \tag{A6}$$

where $\Omega_0 = \frac{\mu_1\mathcal{E}^0_{\rm IR}}{\hbar}$ is the Rabi frequency corresponding to the peak IR intensity. Substituting Eqs. (A6) into Eqs. (A3) and (A4), we get the time- and delay-dependent state amplitude:

$$C_{2p}(t,\tau) = \begin{cases} C^0_{2p}\cos\left[\frac{\Omega_0}{4\omega_1}\left(\omega_1 t + n\sin\frac{\omega_1\tau}{n} + n\sin\frac{\omega_1(t-\tau)}{n}\right)\right], & 0 \leqslant t \leqslant \frac{\pi n}{\omega_1}+\tau, \\ C^0_{2p}\cos\left[\frac{\Omega_0}{4\omega_1}\left(n\pi + \omega_1\tau + n\sin\frac{\omega_1\tau}{n}\right)\right], & \frac{\pi n}{\omega_1}+\tau < t. \end{cases} \tag{A7}$$

Therefore, the final-state amplitude of the $2p$ state as a function of delay is

$$C^f_{2p}(\tau) = C^0_{2p}\cos\left[\frac{\Omega_0}{4\omega_1}\left(n\pi + \omega_1\tau + n\sin\frac{\omega_1\tau}{n}\right)\right]. \tag{A8}$$

APPENDIX B: SQUARE IR PULSE

For the case of the square IR pulse, the time-dependent dipole moment is

$$d(t) = \mu_0[C^*_{1s}(t)C_{2p}(t)e^{-i\omega_0 t} + \text{c.c.}], \tag{B1}$$

where $C_{2p}(t)$ is the $2p$ state amplitude written in Eqs. (8) and (9), and μ_0 is the dipole transition matrix element of $1s$-$2p$. Since the XUV is weak, the ground-state amplitude C_{1s} is set to 1 at all times, and the dipole moment simplifies to

$$d(t) = 2\mu_0\text{Im}[C_{2p}(t)]\sin(\omega_0 t). \tag{B2}$$

When the XUV overlaps the IR pulse, the Fourier transform of the dipole moment is

$$\tilde{d}(\omega) = \frac{2\mu_0 \mathrm{Im}\left[C_{2p}^0\right]}{\sqrt{2\pi}} \left\{ \int_0^{\tau_2} \cos\frac{\Omega t}{2} \sin(\omega_0 t) e^{-i\omega t} dt + \int_{\tau_2}^{\infty} \cos\frac{\Omega \tau_2}{2} \sin(\omega_0 t) e^{-i\omega t} e^{-\alpha t} dt \right\}. \tag{B3}$$

Since we are only interested in the response near ω_0 (and not $-\omega_0$), we keep only the resonant $e^{i\omega_0 t}$ term and obtain

$$\begin{aligned} \tilde{d}(\omega) = \frac{\mu_0 \mathrm{Im}\left[C_{2p}^0\right]}{\sqrt{2\pi} i} \Bigg\{ & \frac{\tau_1 + \tau_0}{2} e^{-\frac{i}{2}(\Delta + \frac{\Omega}{2})(\tau_1 + \tau_0)} \mathrm{sinc}\left[\frac{\tau_1 + \tau_0}{2} \left(\Delta + \frac{\Omega}{2} \right) \right] \\ & + \frac{\tau_1 + \tau_0}{2} e^{-\frac{i}{2}(\Delta - \frac{\Omega}{2})(\tau_1 + \tau_0)} \mathrm{sinc}\left[\frac{\tau_1 + \tau_0}{2} \left(\Delta - \frac{\Omega}{2} \right) \right] + \frac{\alpha - i\Delta}{\alpha^2 + \Delta^2} e^{-\alpha(\tau_1 + \tau_0)} e^{-i\Delta(\tau_1 + \tau_0)} \cos\frac{\Omega(\tau_1 + \tau_0)}{2} \Bigg\}, \end{aligned} \tag{B4}$$

where $\Delta = \omega - \omega_0$ and $\tau_1 = -(\tau + \frac{\tau_0}{2})$. If the XUV pulse is approximated as a δ function $\mathcal{E}(t) = A\delta(t)$, then the response function is

$$\begin{aligned} \tilde{S}(\omega, \tau) = \frac{A\mu_0}{\pi} \mathrm{Im}\left[C_{2p}^0\right] \Bigg\{ & \frac{\tau_1 + \tau_0}{2} \mathrm{sinc}\left[(\tau_1 + \tau_0) \left(\Delta + \frac{\Omega}{2} \right) \right] + \frac{\tau_1 + \tau_0}{2} \mathrm{sinc}\left[(\tau_1 + \tau_0) \left(\Delta - \frac{\Omega}{2} \right) \right] \\ & + \cos\frac{\Omega(\tau_1 + \tau_0)}{2} e^{-\alpha(\tau_1 + \tau_0)} \mathrm{Re}\left[\frac{\alpha - \mathrm{i}\Delta}{\alpha^2 + \Delta^2} e^{-\mathrm{i}\Delta(\tau_1 + \tau_0)} \right] \Bigg\}. \end{aligned} \tag{B5}$$

Similarly, when the XUV is leading the IR pulse, the $2p$ state amplitude is written in Eq. (9). The Fourier transform of the dipole moment can be written as

$$\begin{aligned} \tilde{d}(\omega) = \frac{\mu_0 \mathrm{Im}\left[C_{2p}^0\right]}{\sqrt{2\pi} i} \Bigg\{ & \tau_1 e^{-\frac{i}{2}\Delta\tau_1} \mathrm{sinc}\frac{\Delta\tau_1}{2} + \frac{\tau_0}{2} e^{-i\Delta\tau_1} e^{-\frac{i}{2}(\Delta + \frac{\Omega}{2})\tau_0} \mathrm{sinc}\left[\frac{\tau_0}{2} \left(\Delta + \frac{\Omega}{2} \right) \right] \\ & + \frac{\tau_0}{2} e^{-i\Delta\tau_1} e^{-\frac{i}{2}(\Delta - \frac{\Omega}{2})\tau_0} \mathrm{sinc}\left[\frac{\tau_0}{2} \left(\Delta - \frac{\Omega}{2} \right) \right] + \frac{\alpha - i\Delta}{\alpha^2 + \Delta^2} e^{-\alpha(\tau_0 + \tau_1)} e^{-i\Delta(\tau_0 + \tau_1)} \cos\frac{\Omega\tau_0}{2} \Bigg\} \end{aligned} \tag{B6}$$

and the response function is

$$\begin{aligned} \tilde{S}(\omega, \tau) = \frac{A\mu_0}{\pi} \mathrm{Im}\left[C_{2p}^0\right] \Bigg\{ & \tau_1 \mathrm{sinc}(\Delta\tau_1) + \frac{\tau_0}{2} \cos\left[\Delta\tau_1 + \frac{\tau_0}{2} \left(\Delta + \frac{\Omega}{2} \right) \right] \mathrm{sinc}\left[\frac{\tau_0}{2} \left(\Delta + \frac{\Omega}{2} \right) \right] \\ & + \frac{\tau_0}{2} \cos\left[\Delta\tau_1 + \frac{\tau_0}{2} \left(\Delta - \frac{\Omega}{2} \right) \right] \mathrm{sinc}\left[\frac{\tau_0}{2} \left(\Delta - \frac{\Omega}{2} \right) \right] + \cos\frac{\Omega\tau_0}{2} e^{-\alpha(\tau_0 + \tau_1)} \mathrm{Re}\left[e^{-i\Delta(\tau_0 + \tau_1)} \frac{\alpha - i\Delta}{\alpha^2 + \Delta^2} \right] \Bigg\}. \end{aligned} \tag{B7}$$

[1] E. Goulielmakis, Z.-H. Loh, A. Wirth, R. Santra, N. Rohringer, V. S. Yakovlev, S. Zherebtsov, T. Pfeifer, A. M. Azzeer, M. F. Kling *et al.*, Nature (London) **466**, 739 (2010).

[2] A. Wirth, M. T. Hassan, I. Grgura, J. Gagnon, A. Moulet, T. T. Luu, S. Pabst, R. Santra, Z. A. Alahmed, A. M. Azzeer *et al.*, Science **334**, 195 (2011).

[3] A. McPherson, G. Gibson, H. Jara, U. Johann, T. S. Luk, I. A. Mclntyre, K. Boyer, and C. K. Rhodes, J. Opt. Soc. Am. B **4**, 595 (1987).

[4] M. Ferray, A. L'Huillier, X. F. Li, L. A. Lomreé, G. Mainfray, and C. Manus, J. Phys. B **21**, L31 (1988).

[5] M. Hentschel, R. Kienberger, C. Spielmann, G. a. Reider, N. Milosevic, T. Brabec, P. Corkum, U. Heinzmann, M. Drescher, and F. Krausz, Nature (London) **414**, 509 (2001).

[6] P. M. Paul, E. S. Toma, P. Breger, G. Mullot, F. Aug, P. Balcou, H. G. Muller, and P. Agostini, Science **292**, 1689 (2001).

[7] M. Schultze, E. M. Bothschafter, A. Sommer, S. Holzner, W. Schweinberger, M. Fiess, M. Hofstetter, R. Kienberger, V. Apalkov, V. S. Yakovlev *et al.*, Nature (London) **493**, 75 (2013).

[8] H. Timmers, N. Shivaram, and A. Sandhu, Phys. Rev. Lett. **109**, 173001 (2012).

[9] Z.-H. Loh and S. R. Leone, J. Phys. Chem. Lett. **4**, 292 (2013).

[10] M. Tarana and C. H. Greene, Phys. Rev. A **85**, 013411 (2012).

[11] S. Pabst, A. Sytcheva, A. Moulet, A. Wirth, E. Goulielmakis, and R. Santra, Phys. Rev. A **86**, 063411 (2012).

[12] M. Holler, F. Schapper, L. Gallmann, and U. Keller, Phys. Rev. Lett. **106**, 123601 (2011).

[13] M. Chini, B. Zhao, H. Wang, Y. Cheng, S. X. Hu, and Z. Chang, Phys. Rev. Lett. **109**, 073601 (2012).

[14] S. Chen, M. J. Bell, A. R. Beck, H. Mashiko, M. Wu, A. N. Pfeiffer, M. B. Gaarde, D. M. Neumark, S. R. Leone, and K. J. Schafer, Phys. Rev. A **86**, 063408 (2012).

[15] S. Chen, M. Wu, M. B. Gaarde, and K. J. Schafer, Phys. Rev. A **87**, 033408 (2013).

[16] W.-C. Chu and C. D. Lin, Phys. Rev. A **87**, 013415 (2013).

[17] X. Wang, M. Chini, Y. Cheng, Y. Wu, X.-M. Tong, and Z. Chang, Phys. Rev. A **87**, 063413 (2013).

[18] A. N. Pfeiffer and S. R. Leone, Phys. Rev. A **85**, 053422 (2012).

[19] T. Brabec, *Strong Field Laser Physics* (Springer, New York, 2008).

[20] M. Gavrila, *Atoms in Intense Laser Fields* (Academic Press, Boston, 1992).
[21] M. B. Gaarde, C. Buth, J. L. Tate, and K. J. Schafer, Phys. Rev. A **83**, 013419 (2011).
[22] See, for instance, the discussion of the Bloch-Siegert shift (a low-order correction to the RWA) in [24].
[23] M. Scully, *Quantum Optics* (Cambridge University Press, Cambridge, UK, 1997).
[24] L. Allen and J. Eberly, *Optical Resonance and Two-Level Atoms* (Courier Dover Publications, New York, 1987).
[25] M. Wu, S. Chen, K. J. Schafer, and M. B. Gaarde, Phys. Rev. A **87**, 013828 (2013).
[26] C. Ott, A. Kaldun, P. Raith, K. Meyer, M. Laux, J. Evers, C. H. Keitel, C. H. Greene, and T. Pfeifer, Science **340**, 716 (2013).
[27] L. Argenti, R. Pazourek, J. Feist, S. Nagele, M. Liertzer, E. Persson, J. Burgdörfer, and E. Lindroth, Phys. Rev. A **87**, 053405 (2013).
[28] Y. Wu and X. Yang, Phys. Rev. Lett. **98**, 013601 (2007).
[29] J. C. A. Barata and W. F. Wreszinski, Phys. Rev. Lett. **84**, 2112 (2000).